

Temperature Field Analysis and Process Control Strategies for MgO Single Crystal Production Using Adaptive Neuro-Fuzzy Inference System

Tie Li^{*}, Zhen Wang and Ninghui Wang

School of Electrical Engineering, Dalian University of Technology, China

Abstract: To grow high-purity and large sizes MgO single crystals with twin-electrode DC submerged arc furnace requires that the temperature distribution be well understood and the processing temperature be precisely controlled. For the complexity of the production of MgO single crystals and the difficulty to measure the temperature inside the furnace, the temperature distribution was studied by using finite element method (FEM), and the temperature control was realized by the process control strategies with adaptive neuro-fuzzy inference system (ANFIS). Experiments were carried out to verify the effectiveness of the method. The result of experiments indicated that using the adaptive neuro-fuzzy control system can improve the quality and the quantity of the MgO single crystal production.

Keywords: Finite element analysis, twin-electrode DC submerged arc furnace, temperature field, ANFIS.

1. INTRODUCTION

The ability of the twin-electrode DC submerged arc furnace to process fines, its increased power efficiency, and its lower electrode consumption have made it popular in crystal growth since its introduction in the late 1970s [1]. The twin-electrode DC submerged arc furnace can easily generate temperature up to 3600°C in a short time. Because Magnesium oxide is well known refractory material which has very high melting points, nowadays using twin-electrode DC submerged arc furnace has become the main method applied to grow large magnesium oxide (MgO) single crystals.

The process of MgO single crystals production can be divided into three stages. The first stage is meltdown stage. In this stage the fundamental task is to get desired size of molten pool in MgO powder. In order to supply sufficient electric power for the rapid melting of MgO, the DC voltage of the convertor should be high and the gap between the electrodes should be small. The second stage is refining stage. In this stage the main work is to keep the stability of the molten pool and refine the MgO melt, so the DC voltage should be stepped-down and the gap between the electrodes should be increased. The third stage is crystallization stage. In this stage the core job is to build a relatively stable temperature gradient for the crystal growth. In order to decrease the supply of electric power for the growth of MgO single crystals, the DC voltage should be stepped-down and the gap between the electrodes should be reduced. The supply of the electric power will be shut down until the temperature in the twin-electrode DC submerged arc furnace reach about 2200°C.

With the development of computing power and numerical techniques, the computer modeling of global heat transfer, defect dynamics, and three-dimensional (3D) phenomena for crystal growth has made significant progresses [2]. Finite element method (FEM) was used to predict the temperature distribution.

To keep the stability of the molten pool and build proper temperature gradient in the twin-electrode DC submerged arc furnace is crucial to grow high-purity MgO single crystals with large sizes. For the process of the MgO melting is complicated, and the mechanism of single crystals growth is not clearly known, there are a lot of uncertain factors in the production of MgO single crystals. There have been quite a few researches done both in modeling and simulation of the steel making furnace by the use of conventional and intelligent methods such as fuzzy logic (FL), artificial neural networks (ANN) and neuro-fuzzy systems, an amalgamation of FL and ANN [3]. However, the process of production of MgO single crystals is quite different from steel making. It is necessary to build a temperature controller with intelligent methods such as adaptive neuro-fuzzy inference system (ANFIS) for the twin-electrode DC submerged arc furnace.

For the complexity of the production of MgO single crystals and the difficulty to measure the temperature inside the furnace, in this paper, firstly finite element method (FEM) was used to study the temperature field distributions, and then a temperature controller with adaptive neuro-fuzzy inference system (ANFIS) was developed based on the result of the study of FEM and practical experiences. When the temperature in the twin-electrode DC submerged arc furnace was changed, the controller would regulate the positions of three-phase electrodes and the voltage of the power simultaneously. The result of experiments indicated that using the adaptive neuro fuzzy control system can improve the quality and the quantity of the MgO single crystal production, and through the control of the furnace current, the power quality was improved including power impact and harmonic currents.

^{*}Address correspondence to this author at the School of Electrical Engineering, Dalian University of Technology, China;
Tel: +86-411-84706489; Fax: +86-411-84706489; E-mails: listeel@yeah.net

2. ANALYSIS OF THE TEMPERATURE DISTRIBUTION OF TWIN-ELECTRODE DC SUBMERGED ARC FURNACE

2.1. Mathematic Model of Twin-Electrode DC Submerged Arc Furnace

The electric arc is the main thermal source of the twin-electrode DC submerged arc furnace. The V-A characters of the arc can be expressed as

$$U_f = U_{xh} + I_f R \quad (1)$$

where U_f is arc voltage; I_f is arc current; R is arc equivalent resistance;

R can be calculated by

$$R = \rho k d / (k \pi d^2) \quad (2)$$

where ρ is resistivity of submerge-arc determined by experiments; d is diameter of the electrode; the arc length is $k d$, k is proportionality coefficient; Then R can be seen as the resistance of the arc whose length is $k d$, and section area is $k \pi d^2$.

Given equation [1] through [2],

$$U_f = U_{xh} + b l \quad (3)$$

In equation (3), l is arc length, b is arc voltage coefficient, determined by experiments; U_{xh} is extinction voltage, determined by the material of electrode, about 14V.

It is assumed that the arc distribution is normal. When one arc goes from the center of one electrode and reaches to the other electrode, it forms an arc spot on the surface of the electrode. The heat flux can be expressed as

$$q(r) = q_m \cdot e^{-kr^2} \quad (4)$$

where q_m is the heat flux of the arc spot; k is the distance coefficient; r is the distance from the arc spot [4].

Assumed that the radius of arc spot $rH=R+2l$, and the heat flux $q(rH)=0.05q_m$, then $k=3(R+2l)^{-2}$. The energy distribution of any spot can be expressed as

$$q_1(r) = \frac{3k_1 P_1'}{\pi(R+2l)^2} \cdot e^{\left(\frac{-3r^2}{(R+2l)^2}\right)} \quad (5)$$

where P_1' is the arc power of one electrode; k_1 is the thermal conductance coefficient.

The molten pool resistance 'r' is also a significant parameter for modeling the twin-electrode DC submerged arc furnace. For a spot whose coordinate is (x, y, z), assumed that the area of the spot is $dx \times dy$, the conductance can be described as

$$G' = dx dy / (\rho d)$$

where d is distance between the spot and the center of the electrode.

The current passed through the spot can be described as

$$i = I \times G' / G$$

Obviously, The molten pool resistance 'r2' can be obtained by

$$G = \iiint G' dx dy dz \quad (6)$$

The electric energy of the spot inside the molten pool is given as

$$q_2(x, y, z) = i^2 r' = I^2 \cdot G' / G^2 \quad (7)$$

The energy distribution in molten pool has the form

$$Q = q_1 + q_2$$

where q_1 is calculated according to equation (5) and q_2 is calculated according to equation (7).

The equation of temperature distribution in molten pool is written as

$$\frac{\partial}{\partial x} \left(c \frac{\partial T}{\partial x} \right) + \frac{\partial}{\partial y} \left(c \frac{\partial T}{\partial y} \right) + \frac{\partial}{\partial z} \left(c \frac{\partial T}{\partial z} \right) + Q = 0 \quad (8)$$

where T is temperature, c is conductivity coefficient.

2.2. Thermal Analysis by FEM

A finite element (FE) thermal model was developed to determine temperature distribution in an twin-electrode DC submerged arc furnace during normal operation [5]. The commercial simulation software ANSYS was used to carry out the FE simulation. The mesh of the model used for 3D simulations was shown in Fig. (1). The information for the analysis, mainly including geometry, working conditions and process parameters were presented in Table 1. The thermal conductivity of MgO powder was assigned as a function of temperature which was presented in Table 2. Fig. (2) showed the simulated temperature contours for transverse cross-section of the twin-electrode DC submerged arc furnace, and Fig. (3) showed the simulated temperature contours for longitudinal cross-section of the twin-electrode DC submerged arc furnace. Fig. (4) showed the molten pool near the electrodes during preparation process of MgO single crystal.

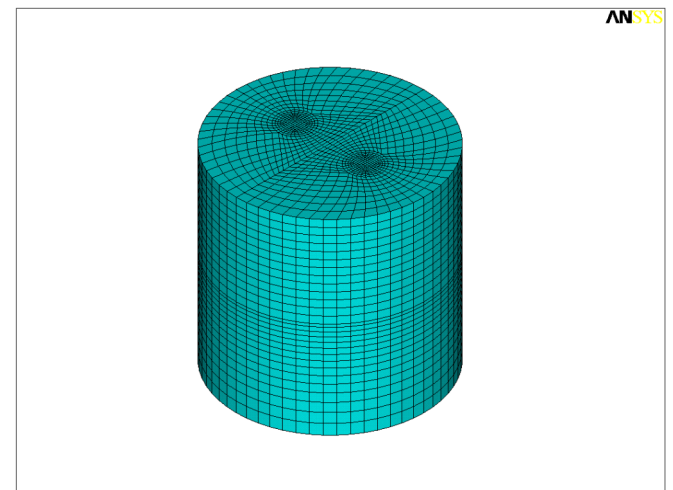


Fig. (1). Finite element mesh for thermal analysis of twin-electrode DC submerged arc furnace.

Table 1. Characteristics of Work Electrodes and MgO Single Crystal Furnace

Characteristic	Value
Electrode length, m	2.4
Electrode diameter, m	0.35
The distance between electrodes center (mm)	750
Voltage of the output of DC convertor, V	72
DC current passing the electrodes, A	6500
Temperature of the furnace atmosphere, K	400
Ambient temperature, K	398
Convection coefficient for furnace wall, W m ⁻² K ⁻¹	110
Convection coefficient for ambient air, W m ⁻² K ⁻¹	10

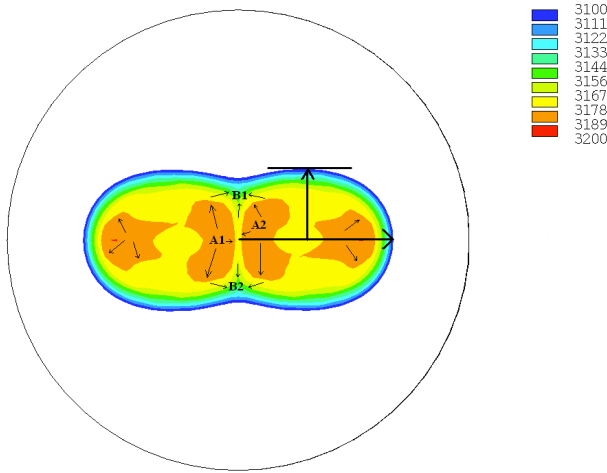


Fig. (2). Simulated temperature contours for transverse cross-section of the furnace, the arrow indicated the direction of the mass transfer.

Some conclusions can be drawn from the comparison between simulated results and practical work.

Table 2. Thermal Conductivity of MgO Powder

Phase	Temperature (K)	Cp (J•(mol•K) ⁻¹)	H _T ⁰ - H ₂₉₈ ⁰ (J•mol ⁻¹)	σ(Ω ⁻¹ •cm ⁻¹)	
Solid Powder	300	37.203	74	Insulated	
	600	47.630	13280		
	1000	50.949	33104		
	1400	52.763	53865		
	1800	54.249	75273		
	2200	55.621	97250		
	2600	56.943	119763		
Crystals	2800	57.594	131217	20.9	
	3000	58.240	142801		
Liquid	3098	58.556	148524		22.7
	3098	60.668	225928		
	3200	60.668	232116		
	3400	60.668	244229		
	3533	60.668	252318	25.7	
				26.5	

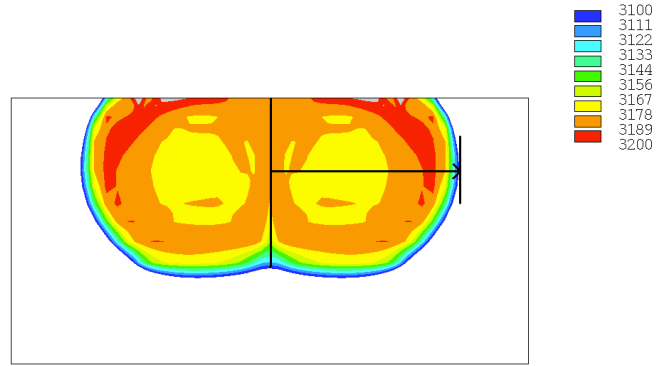


Fig. (3). Simulated temperature contours for longitudinal cross-section of the furnace.



Fig. (4). Photograph of molten pool during melting process.

- A) The temperature was highest under the electrodes, and the temperature gradient outside the regions quickly descended with increasing distance. The MgO powder got the best smelted here, but the dissipation was also highest in these regions.
- B) In the regions of A1 and A2, the temperature gradient was the steepest. The material in the molten pool was

driven outward by the temperature difference. The arrow indicated the direction of the mass transfer. For the melting point of impurities were lower, they melt to liquid in advance of MgO powder and moved up to the surface of the molten pool. This made the surface of the molten pool mainly formed by impurities. The regions of A1 and A2 were the hot spots of the molten pool, the MgO powder was well smelted and refined here.

- C) In the regions of B1 and B2, the temperature gradient was gentle. The arrow indicated the direction of the mass transfer. For the force of temperature difference was low, these regions were cold spots of the molten pool. Here the MgO powder could not get well smelted and refined.
- D) The temperature gradient descended with increasing depth in the interior of the molten pool. There was a temperature peak in the central of the region, but the temperatures at the periphery of the molten pool were low and very closed. This indicated that the fluidity of the melt was impaired with increasing depth in the interior of the molten pool.

3. ANFIS MODELING

An adaptive neuro-fuzzy controller for the preparation of MgO single crystal was constructed based on the results of the study of FEM and practical experiences. ANFIS is a fuzzy system which is often used in classification, modeling and solving control problems. It is based on Takagi and Sugeno model fuzzy if-then rules representation [6], which is different from commonly used fuzzy logic controllers [7,8]. The consequent part of the rule is a function of input variables. The inference mechanism of ANFIS is mathematically expressed by the set of the rules. The schematic diagram of the system was shown in Fig. (5).

The control of the electrodes movements and the regulation of the output voltage of the DC convertor were directly related to the arc current between the electrodes and

the MgO powder. It was central to the control system of the twin-electrode DC submerged arc furnace and affected the temperature gradient distribution in the furnace.

In the Fig. (5), T_r was the set value of temperature, and T_a was the measured value of temperature of the furnace. Subtraction of T_a from T_r yielded ΔT , which was known as deviation signal, i.e., the difference between the set value and the actual value of temperature. I_A was the operation current of the system. The fuzzy controller had two input terminals, ΔT and I_A . S_A and U_A were the outputs of the fuzzy controller, which were converted to analog by D/A converter and keeper. U_A was used to adjust the output voltage of the DC convertor and S_A was used to regulate the movements of the electrodes [9].

A total of 350 data sets were obtained from the results of the study of FEM and practical experiences. Among them a total of 300 data sets were selected for the purpose of training in ANFIS and the rest 50 data sets were selected for testing purposes after the training was completed in order to verify the accuracy of the predicted values [10].

Next, the genetic-oriented clustering method was applied to the training data sets. The cluster centers determined the number of the fuzzy sets and the parameters (mean values) μ of the membership functions of the antecedent part, as well as the number of fuzzy rules of the Sugeno-type FIS. The standard deviation σ was computed as $\sigma = r_a \cdot 8^{-0.5}$ for all membership functions, where r_a was the radius of influence [11]. The number of the resulted clusters for $r_a = 0.4$ was seven. As a result, each input variable was characterized by seven fuzzy sets with the linguistic values. The consequent parameters of each rule of the Sugeno-type FIS were determined by using the linear least-squares algorithm [12]. The rule base obtained through the genetic-oriented clustering approach consisted of twenty-four rules, shown in Table 3.

The next step is the training process that aims at tuning the fuzzy inference system. Fig. (6) shows the final

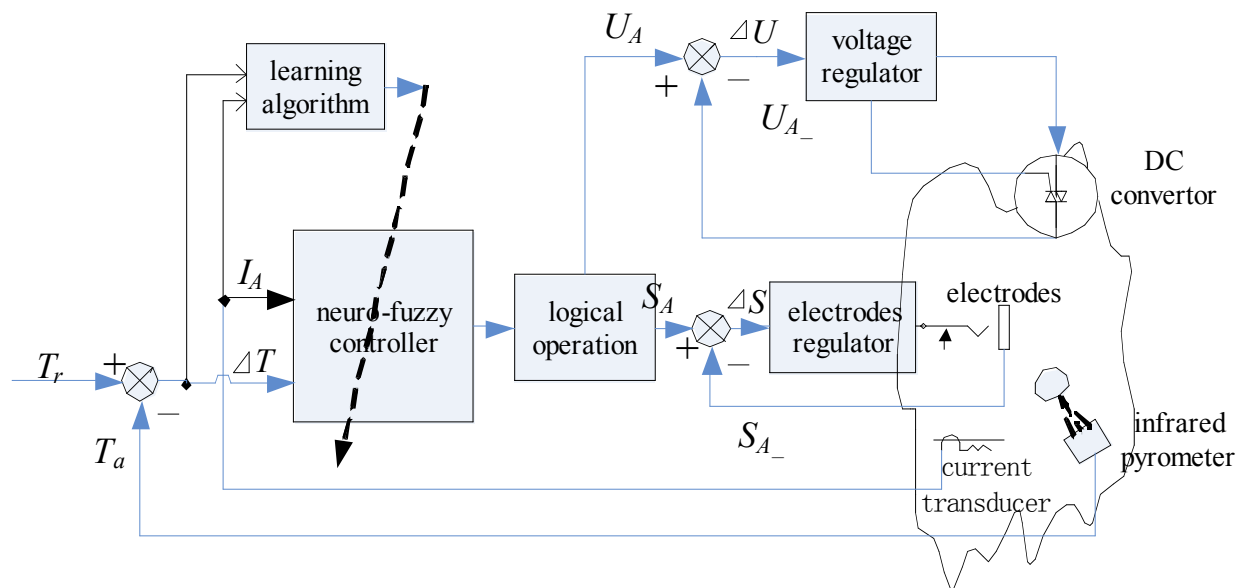


Fig. (5). Schematic diagram of the adaptive neuro-fuzzy inference system.

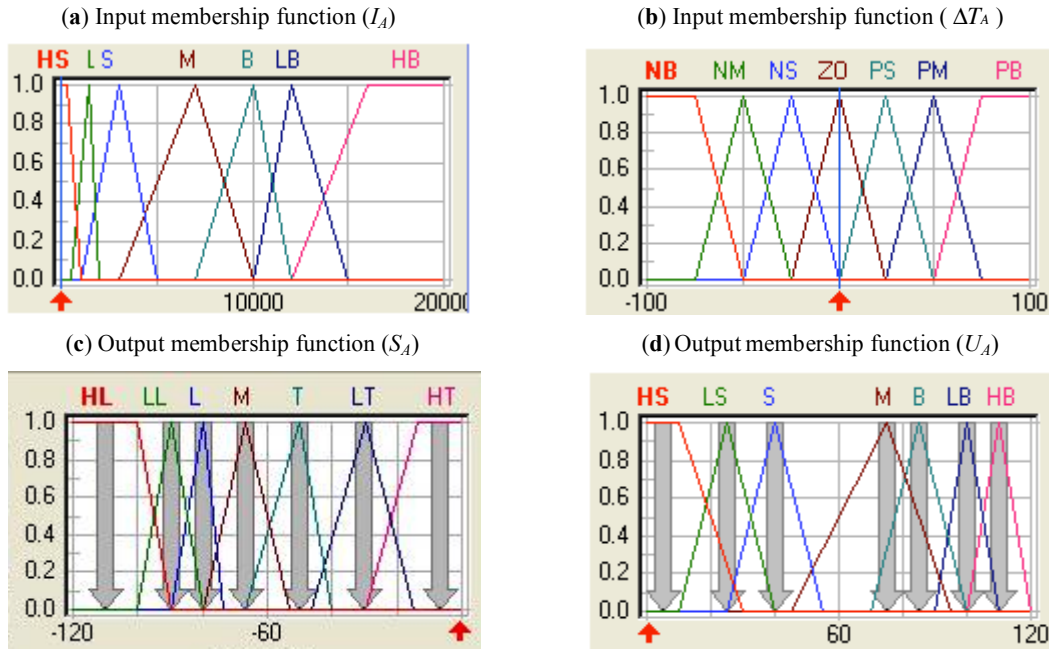


Fig. (6). The final membership functions for input and output after training.

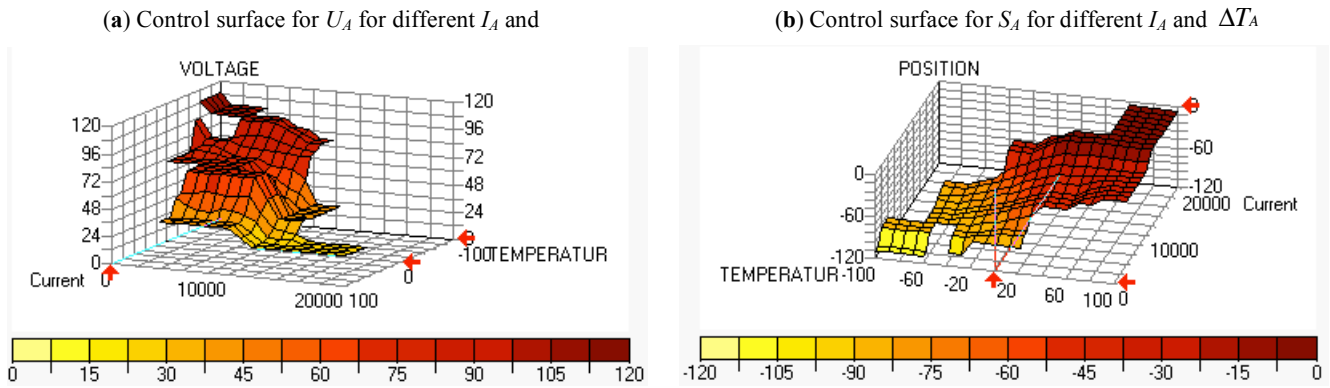


Fig. (7). Three-dimensional plot indicative of the relationship between inputs and outputs.

membership functions derived from the training system. In contrast to the first input, there is a considerable change in the final membership functions concerning the second input, since the supports of all fuzzy sets are broadened. Fig. (7) depicts a three-dimensional plot that represents the mapping from the furnace current and the temperature error to the electrodes position and the output voltage of the DC convertor. The surface has a good continuity as it is normally expected from a Sugeno-fuzzy controller.

Table 3. Fuzzy Rule Base

<p>(1) If I_A is HS and ΔT_A is NB then S_A is HL and U_A is HB or</p> <p>(2) If I_A is HS and ΔT_A is NM then S_A is LL and U_A is LB or</p> <p>(3) If I_A is HS and ΔT_A is NS then S_A is L and U_A is B or</p> <p>..... or</p> <p>(4) If I_A is HB and ΔT_A is PB then S_A is NB and U_A is HS</p>
--

Fig. (8) compared the current characters of the preparation system for different control systems with experiments. The capability of restraining the disturbances of current was greatly improved by using adaptive control

system instead of PID control system, which can be proved by the fact that with ANFIS the magnitude of arc current fluctuation was only about one of fourteen with PID. Fig. (8) also showed that the current fluctuated wildly at the beginning, but trended towards stabilization with time going by. This indicated that the adaptive neuro-fuzzy controller need to be optimized at the beginning section of the preparation.

The temperatures of the furnace external shell measured by the adaptive neuro-fuzzy controller were showed in Fig. (9). The temperature rose slowly with time going by, and tended to be stable at last. The maximum temperature of the furnace external shell was lower than 750°C, this was in good agreement with the result estimated by FEM and avoided the shell overheating.

4. EXPERIMENTS AND DISCUSSION

To verify the effectiveness of the adaptive neuro-fuzzy controller for the preparation of MgO single crystal, experiments were carried out in Liaoning Zhongda Superconducting Material CO., Ltd. The controller comprised a industrial PC which equipped with a single PXI-

6259 card, a Minolta/Land Cyclops 152 infrared pyrometer, one Halmar current transducers (Lem-Dynamp Corp., Grove City, Ohio), one voltage sensor and a position measuring potentiometer. The NI software LabView was installed on the PC. The analog output from sensors were conditioned and fed into analog input channels of the PXI-6259. Controlled by fuzzy Vi of the NI software LabView, the control signal was converted to an analog signal and sent out using one of the D/A channels on the PXI-6259 card to regulate the positions of two electrodes and the voltage of the power [13,14].

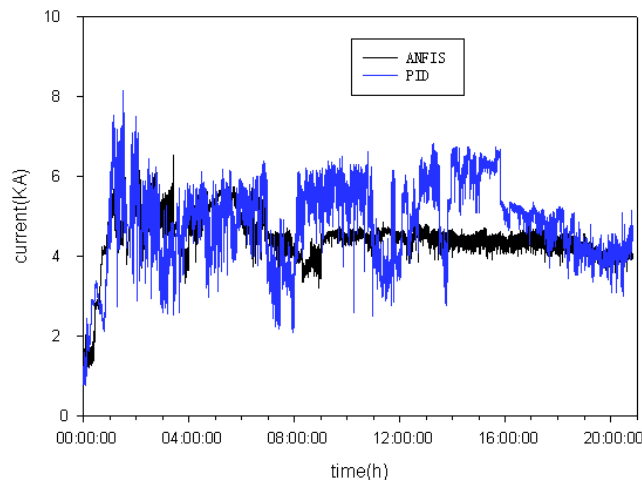


Fig. (8). Comparison of working current between using adaptive neuro-fuzzy inference system and PID control system.

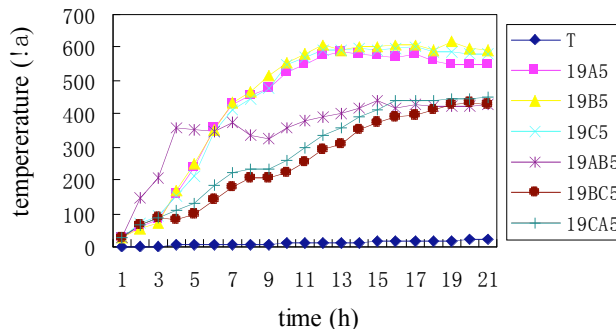


Fig. (9). Distribution diagram of the temperature of temperature-measured points on the external shell of the furnace using adaptive neuro-fuzzy inference system.

Numerous growth experiments had been performed using the MgO powder. MgO single crystals had been grown by the use of the adaptive neuro-fuzzy inference system. The preferential direction of the obtained large crystals was the (1 0 0) direction, which was validated by previous work.

X-ray powder diffraction (XRD, D/Max 2400, Rigaku, by a diffractometer equipped with the graphite-monochromatized $\text{CuK}\alpha$ radiation) was employed to analyze the crystalline structure of large MgO crystals in the 2θ angles ranging from 2° to 85° after the obtained MgO single crystals were ground into ultra-fine powders.

The XRD pattern of powders of the large MgO single crystal grown by the adaptive neuro-fuzzy inference system was shown in Fig. (10). All the reflections of the sample can

be readily indexed as a pure cubic phase of the MgO single crystal, which were identical to the reported data in the JCPDS cards (45-0946). The ideal intensity ratio between (220) and (200) was about 0.4, whereas the measured ratio in this study is smaller than 0.1. The intensity from the (220) diffraction is strongly depressed.

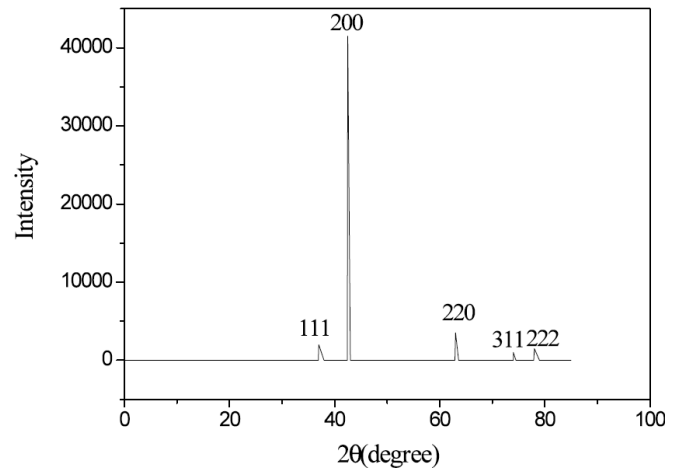


Fig. (10). XRD pattern of the large MgO single crystal: measured by scan speed $6^\circ/\text{min}$ and step interval is 0.020° .

Fig. (11) presents optical absorption spectra of large MgO single crystals in UV-VIS-NIR wavelength at room temperature. MgO single crystal possesses a steep absorption edge in the UV region (about 280nm), which means that the strong photoabsorption of these crystals occurs only at wavelengths shorter than 280 nm.

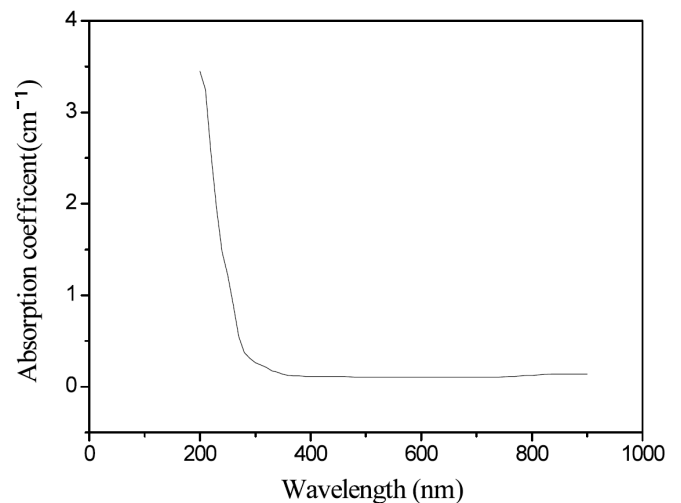


Fig. (11). Optical absorption spectra of MgO single crystals in the UV-VIS-NIR region.

The ICP-AES analytical technique is a non-destructive analytical method which uses no chemicals for dissolution. It can achieve the detection limits below 0.01 ppm level for most of the impurity elements and it can also be used to trace impurity elements quantity in the crude as well as refined MgO powder. ICP-AES results are summarized in Table 4.

From the table you can see the overall purity of MgO single crystal was increased from 99% to 99.99%. In case of MgO melting, 96% of total Ca, Al, and Fe impurities were removed. On the same lines, the metallic impurities were

reduced by 99% when compared to the initial impurities in crude MgO powder. ICP-AES analysis results of the MgO single crystals showed excellent removal effect of interstitial and metallic impurities due to the fact that the high temperature helped in better vaporization of metallic impurities as well as interstitial gases.

Table 4. ICP-AES Results of the MgO Crystal

Items	Testing Value	ICP Wave-Length	
Impurity	Al	2ppm	396.153
	Ca	32ppm	317.933
	Si	0	251.611
	Fe	18ppm	238.204
	Na	46ppm	589.592
	K	30ppm	766.490

Fig. (12) showed the production of the MgO single crystals. Fig. (13) showed the surface map of the MgO single crystal which had been cut and polished. The average size of the single crystals was about 6-8cm, much bigger than those prepared by manual operation, and the MgO single crystal output rose from 300 kg to 800 kg per heat.



Fig. (12). Photograph of the large MgO single crystal grown using adaptive neuro-fuzzy inference system.

5. CONCLUSIONS

FEM was effective to study the temperature distribution in the preparation process of MgO single crystal. The temperature in the furnace could be precisely estimated according to the time of operation and process parameters by FEM. This would help to study the single crystal growth theory of MgO, and proposed evidences to the process control of preparation of MgO single crystal. Based on the results of the study of FEM and practical experiences, a temperature controller with adaptive neuro-fuzzy inference system (ANFIS) was developed to regulate the positions of two electrodes and the voltage of the power. The result of

experiments proved that using the adaptive neuro fuzzy control system can improve the quality and the quantity of the MgO single crystal production. It indicated that the temperature controller with ANFIS was suitable to control the preparation process of MgO single crystal.

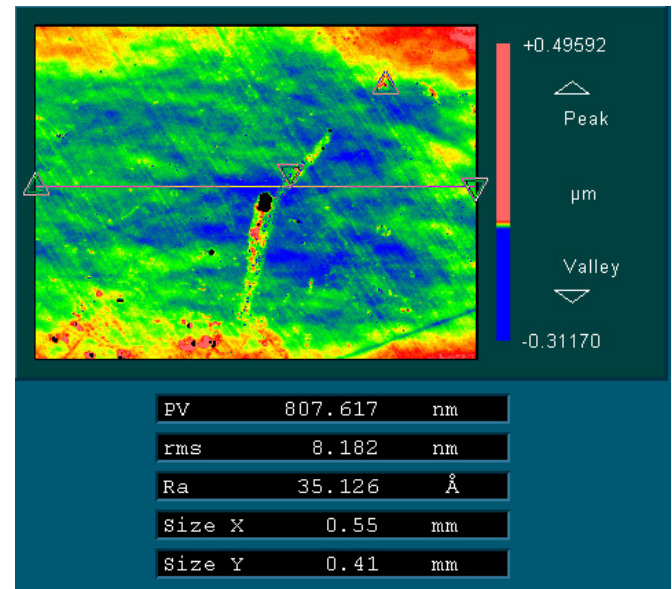


Fig. (13). Surface map of the MgO single crystal after cut and polished.

ACKNOWLEDGEMENTS

This work was financially supported by National Natural Science Foundation of China No.2008AA03A325 and by a Hundred Talents Project of Chinese Academy of Sciences.

REFERENCES

- [1] Xu Zhang. Improved growth technology of large MgO single crystals. *J Cryst Growth* 2006; 292: 505-9.
- [2] Muller G. Challenges in modeling of bulk crystal growth. *J Cryst Growth* 2004; 266: 1-19.
- [3] Manuel. Online estimation of electric arc furnace tap temperature by using fuzzy neural networks. *Eng Appl Artif Intell* 2008; 21: 1001-2.
- [4] Wang F. Fluid Flow Modeling of Arc Plasma and Bath Circulation in DC Electric Arc Furnace. *J Iron Steel Res* 2006; 13: 7-13.
- [5] Kumar A. Comparative leakage field analysis of electromagnetic devices using finite element and fuzzy methods. *Expert Syst Appl* 2010; 27: 3827-34.
- [6] Zheng T, Makram EB. An adaptive arc furnace model. *IEEE Transactions on Power Delivery* 2000; 15: 931-40.
- [7] Jang J-SR. Input selection for ANFIS learning. In *Proceedings of the IEEE International Conference on Fuzzy Systems*. New Orleans, LA, USA 1996.
- [8] Janabi-Sharifi F, Jorjani G. An adaptive system for modelling and simulation of electrical arc furnaces. *Control Engineer Practice* 2009; 17: 1202-19.
- [9] Anupam D, Maiti J. Process control strategies for a steel making furnace using ANN with bayesian regularization and ANFIS. *Expert Systems with Applications* 2010; 37: 1075-85.
- [10] Dinh NQ, Afzulpurkar NV. Neuro-fuzzy MIMO nonlinear control for ceramic roller kiln. *Simulation Modelling Practice and Theory* 2007; 15: 1239-58.
- [11] Ekmekci I, Yetisken Y, Camdali U. Mass balance modeling for electric arc furnace and ladle furnace system in steelmaking facility in Turkey. *J Iron Steel Res* 2007; 14: 1-6.

- [12] Elmas C, Ustun O, Sayan HH. A neuro-fuzzy controller for speed control of a permanent magnet synchronous motor drive. *Expert Syst Appl* 2008; 34: 657-64.
- [13] Horng, JH. Hybrid MATLAB and LabVIEW with neural network to implement a SCADA system of AC servo motor. *Adv Eng Software* 2008; 39: 149-55.
- [14] Huang SN, Tan KK, Lee TH. Adaptive neural network algorithm for control design of rigid-link electrically driven robots. *Neuro computing* 2008; 71: 885-94.

Received: April 11, 2011

Revised: June 2, 2011

Accepted: June 2, 2011

© Li *et al.*; Licensee *Bentham Open*.

This is an open access article licensed under the terms of the Creative Commons Attribution Non-Commercial License (<http://creativecommons.org/licenses/by-nc/3.0/>) which permits unrestricted, non-commercial use, distribution and reproduction in any medium, provided the work is properly cited.